Journal of Solid State Chemistry 182 (2009) 3406–3411

Contents lists available at ScienceDirect

Journal of Solid State Chemistry

journal homepage: www.elsevier.com/locate/jssc

Thermo-Raman spectroscopy *in situ* monitoring study of solid-state synthesis of NiO–Al_2O_3 nanoparticles and its characterization

Anil Vithal Ghule *, Kalyani Ghule, Shin-Hwa Tzing, Tushar H. Punde, Hua Chang, Yong Chien Ling *

Department of Chemistry, National Tsing Hua University, Hsinchu, Taiwan-300, R.O.C

ARTICLE INFO

Article history:
Received 22 May 2009
Received in revised form
6 September 2009
Accepted 14 September 2009
Available online 1 November 2009

Keywords:
Thermogravimetric analysis
Thermo-Raman spectroscopy
In situ monitoring
Nanoparticles
Nickel alumina catalyst
Characterization

ABSTRACT

Hyphenation of thermogravimetric analyzer (TGA) and thermo-Raman spectrophotometer for *in situ* monitoring of solid-state reaction in oxygen atmosphere forming NiO–Al_2O_3 catalyst nanoparticles is investigated. *In situ* thermo-Raman spectra in the range from 200 to 1400 cm^{-1} were recorded at every degree interval from 25 to 800 °C. Thermo-Raman spectroscopic studies reveal that, although the onset of formation is around 600 °C, the bulk $NiAl_2O_4$ forms at temperatures above 800 °C. The X-ray diffraction (XRD) spectra and the scanning electron microscopy (SEM) images of the reaction mixtures were recorded at regular temperature intervals of 100 °C, in the temperature range from 400 to 1000 °C, which could provide information on structural and morphological evolution of NiO–Al_2O_3. Slow controlled heating of the sample enabled better control over morphology and particle size distribution (~20–30 nm diameter). The observed results were supported by complementary characterizations using TGA, XRD, SEM, transmission electron microscopy, and energy dispersive X-ray analysis.

1. Introduction

Nickel alumina (NiO–Al_2O_3) catalysts have gained economic importance, not only for their wide applications in various industrial processes like hydrogenation, dehydrogenation, methanation, amination, petroleum reforming, for treating chloro-organic compound containing wastes etc., but also, for their easy availability, low cost, high activity, high melting point, and strong resistance to acids and alkali [1–5]. Furthermore, nickel alumina based oxides have also developed renewed interest for their potential applications in CO_2 reduction (artificial photosynthesis) [6,7], as electrochromic material in smart windows [8], sensors [9], and as surface layers and toughenings [10]. With this motivation, extensive work on their synthesis using different methods like solid-state reaction [1], impregnation [11], spray pyrolysis [12], microwave [13], oxidation [14], co-precipitation [11], sol–gel [9,15], sonochemistry [16], ion exchange [17] etc., followed by characterization, electrical and optical property, specific activity, and catalyst recovery etc., studies have been carried out. However, it is important to note that thermal activation treatment (calcination or reduction) is an inevitable step during the catalyst preparation, irrespective of the method used, and thus, the researchers have become interested in this study. Furthermore, calcinations temperature, heating rate, surrounding atmosphere, support etc., governs the particle size, aggregation, surface area, specific activity, and structural properties of the catalyst [1,13,18–23]. As a result, increasing interest has been developed to study the structural, chemical, physical properties, and the interaction between supported metal oxide and the support, as a function of metal loading and calcinations temperature. A variety of surface spectroscopic techniques, e.g. X-ray diffraction (XRD) [22], X-ray photoelectron spectroscopy (XPS) [14], ion scattering spectroscopy (ISS), extended X-ray absorption fine structure (EXAFS) [24], and photo acoustic spectroscopy (PAS) [25], Raman spectroscopy [26] etc. have been used to study catalysts. However, Raman spectroscopic studies on NiO–Al_2O_3 catalyst are scarce [27]. On the other hand, conventional thermal analysis techniques have been used for years to study catalyst systems, but these provide limited or indirect information about the structural properties. Thus, there is a need to develop *in situ* monitoring techniques [28], like thermo-Raman spectroscopy (TRS), highlighting its significance for applications in academic and industrial research [29].

In situ monitoring using TRS is an ideal approach in understanding the structural evolution of the material, its characteristic properties and in defining optimum calcination temperature, which is a crucial step in catalyst preparation [28]. However, to the best of our knowledge, no report on TRS study on NiO–Al_2O_3 catalyst exists. Thus, it was of our interest to explore *in situ* monitoring of NiO–Al_2O_3 catalyst formation using TRS. In this study, the NiO–Al_2O_3 catalyst is prepared by solid-state reaction. The thermal process is further monitored by hyphenated TGA–TRS, in which, Raman spectra are recorded continuously at every degree interval. Furthermore, XRD, transmission electron microscopy (TEM), and scanning electron microscopy (SEM) techniques were used to characterize the resultant products.

* Corresponding authors. Fax: 886 3 5711082.
E-mail addresses: anighule@gmail.com (A.V. Ghule), ycling@mx.nthu.edu.tw (Y.C. Ling).

0022-4596/$ - see front matter © 2009 Elsevier Inc. All rights reserved.
doi:10.1016/j.jssc.2009.09.019

2. Experimental

$Ni(CH_3COO)_2 \cdot 4H_2O$ (Showa Chemicals) is hygroscopic, thus it was heated to 80 °C for 1 h to form anhydrous $Ni(CH_3COO)_2$ and then mixed with $Al(OH)_3$ (Riedel-de Haën) (1:2 molar ratio) for solid-state synthesis of $NiO–Al_2O_3$ catalyst.

Hyphenation of thermogravimetric analyzer (TGA, Perkin Elmer TGA6) to thermo-Raman spectrometer and the necessary optical alignment is shown in Fig. 1. TGA was used to record the thermogravimetric-differential thermogravimetric (TG-DTG) thermograms in the temperature range from 25 to 800 °C with a heating rate of 5 °C min^{-1} in a flow of oxygen gas at 20 mL min^{-1}. Flynn and Wanke reported that, oxidizing atmospheres give more severe sintering compared to inert or reducing atmospheres [20], and thus, oxygen as a carrier gas is used in our experiments. The sample in an alumina crucible was pressed gently and mounted on the TGA sample holder. The thermo-Raman spectra were excited by an argon ion laser (514.5 nm, 50 mW, Coherent, Innova 100–15). The scattered light from the sample was collected using 180° back scattering mode, dispersed by a single spectrometer (Spex, 0.5 m) with a resolution of 4 cm^{-1} and detected by a charged coupled device (CCD) camera (Princeton Instruments, 1024 × 1024 pixels) using appropriate CCD exposure time, which enables spectra collection at every degree interval. A Notch filter was used to remove the Rayleigh scattered light. Thermo-Raman spectra were collected continuously without disturbing the sample. Over all, 775 spectra were collected in each set of experiment and checked for their reproducibility during the formation of $NiO–Al_2O_3$ catalyst nanoparticles in solid-state synthesis. Spectral lines generated from the argon lamp were used for calibration. The XRD patterns were obtained using material analysis and characterization (MAC) advanced powder X-ray diffractometer ($CuK\alpha_1$ = 1.54056 Å). Samples for temperature dependent XRD studies were prepared by heating the solid-state mixture at 5 °C min^{-1} in a temperature programmed furnace in air atmosphere. A small portion of each sample was withdrawn at temperature intervals of 100 °C, and stored in airtight glass vials after appropriate natural cooling. TEM (Philips, Tecnai 20) with inbuilt energy-dispersive X-ray analysis (EDS) and SEM (Hitachi-S4700) were also used to characterize the samples.

3. Results and discussion

TG-DTG thermograms (30–800 °C) of solid-state mixture of $Ni(CH_3COO)_2$ and $Al(OH)_3$ (molar ratio 1:2) with oxygen as carrier gas (20 mL min^{-1}) at heating rate of 5 °C min^{-1} are shown in Fig. 2. The solid-state reaction involved is given below:

$$Ni(COOCH_3)_2 + 2Al(OH)_3 \rightarrow NiO–Al_2O_3 + 2(CH_3COOH) + 2H_2O \quad (5)$$

TG thermogram shows three steps of weight loss. The first two weight losses (30–200 °C) correspond to loss of water molecules, either which is absorbed on the sample or due to condensation, and is in agreement with the observed weight loss of 5.8% as against the calculated weight loss of 5.3%. The third sharp weight loss (200–300 °C) can be attributed to the loss of acetate groups from $Ni(CH_3COO)_2$, and also due to condensation of $Al(OH)_3$ losing the water molecule to form $NiO–Al_2O_3$. This can be justified from the fact that decomposition of acetate [29] and dehydration of $Al(OH)_3$ is reported at ~300 °C. Overall observed weight loss in the thermal process is 46% as against the calculated weight loss of 46.3% forming $NiO–Al_2O_3$. On the other hand, DTG thermogram shows endotherms at 85, 102, 187, 228, 300 and 514 °C. The endotherms at 85, 102 and 187 °C correspond to the loss of water molecules, whereas the endotherms at 228 and 300 °C with a shoulder could be attributed to the loss of acetate groups and condensation of $Al(OH)_3$. The endotherm at 514 °C results from a slow and prolonged condensation process forming $NiO–Al_2O_3$.

Dynamic and static thermal processes are important for basic research and technological applications, in determining the characteristic physical and chemical properties of materials as a function of temperature/time. The conventional thermal analysis techniques (thermogravimetric analysis (TGA), differential

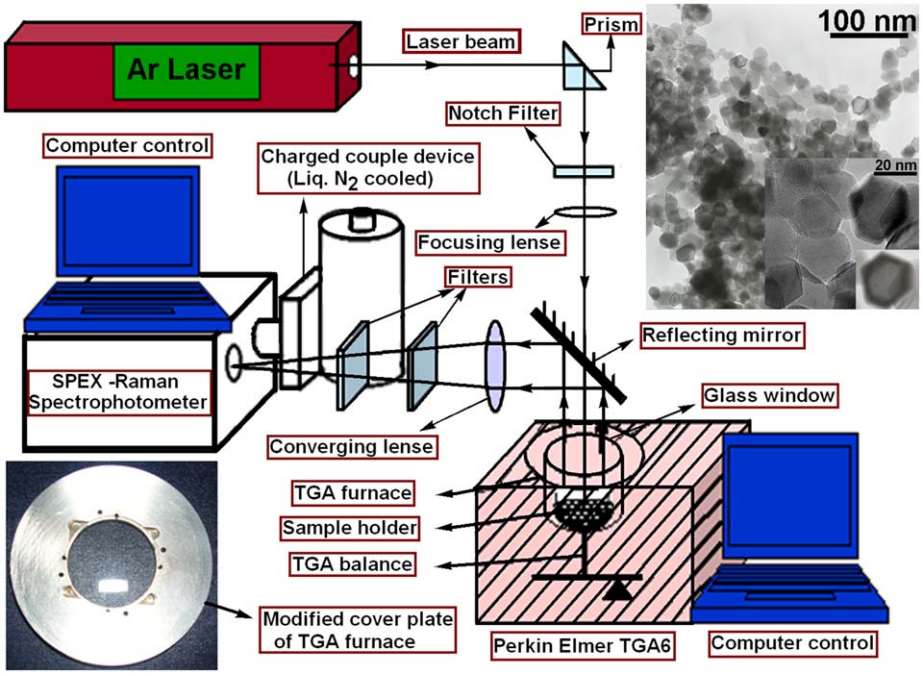

Fig. 1. Schematic showing thermo-Raman spectroscopy setup used for the *in situ* monitoring of solid-state synthesis of $NiO–Al_2O_3$ nanoparticles. Inset shows representative TEM images of solid-state synthesized $NiO–Al_2O_3$ nanoparticles.

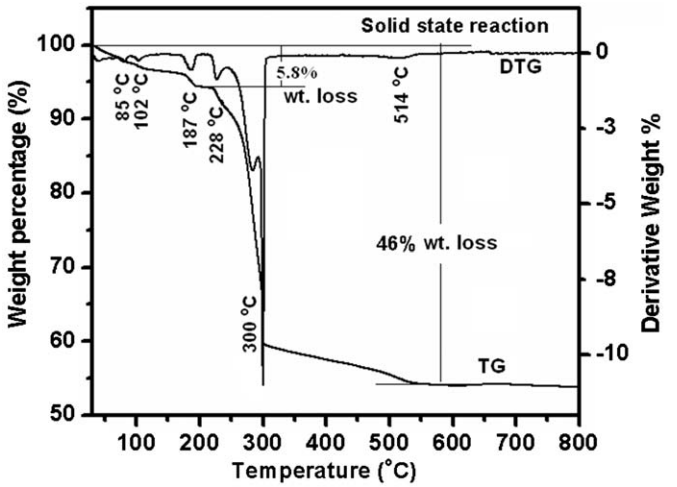

Fig. 2. TG-DTG thermograms of solid-state mixture of $Ni(CH_3COOH)_2$ and $Al(OH)_3$ (molar ratio 1:2) in oxygen atmosphere in the temperature range from 30 to 800 °C and heating rate of 5 °C min^{-1}.

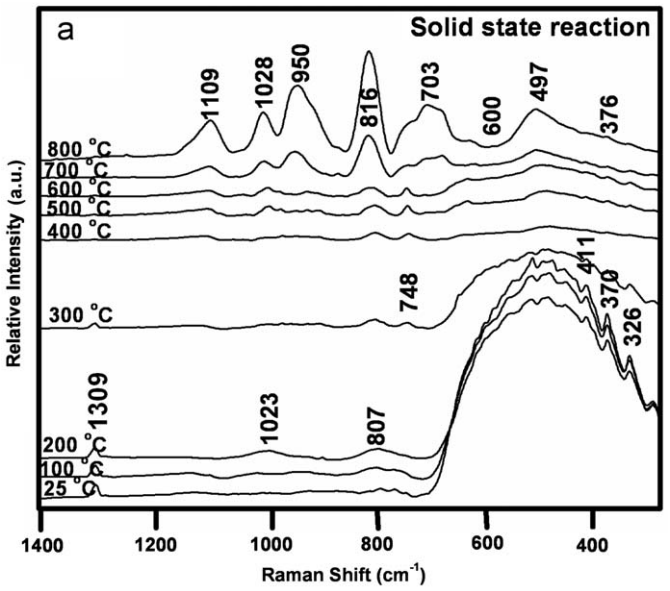

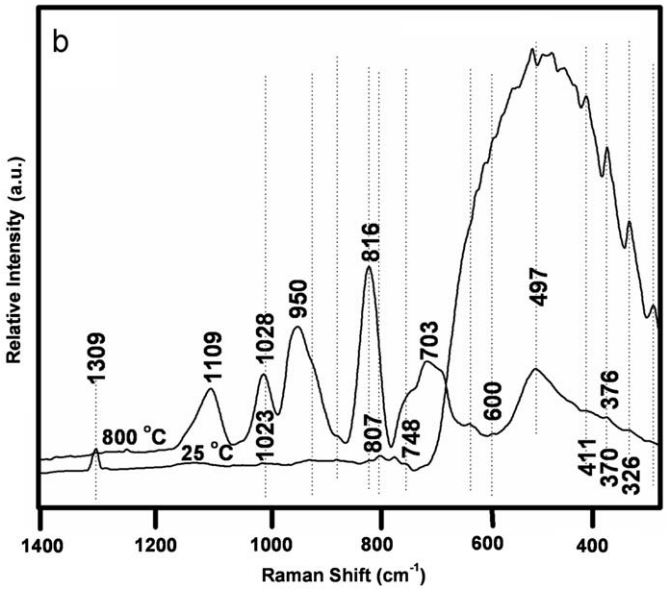

Fig. 3. (a) Thermo-Raman spectra (200–1400 cm^{-1}) of solid-state reaction of $Ni(CH_3COOH)_2$ and $Al(OH)_3$ (molar ratio 1:2) in the temperature range from 25 to 800 °C in oxygen atmosphere with heating rate of 5 °C min^{-1}. (b) Comparison of thermo-Raman spectra obtained at 25 and 800 °C.

thermal analysis (DTA) and differential scanning calorimetry (DSC)) provide information limited to physical properties and indirect information about the identity of the composition and phases evolved. TRS on the other hand, provides structural information and has been exploited by the materials community for characterization of material during dynamic and static thermal processes. The hyphenation of TGA and TRS was first executed in our laboratory, and has been extensively used to study several dynamic thermal processes [29,30].

Although, thermo-Raman spectra at every degree interval were recorded, only representative spectra at regular intervals of 100 °C during the solid-state reaction of $Ni(CH_3COO)_2$ and $Al(OH)_3$ (molar ratio 1:2) in the temperature range from 25 to 800 °C are shown in Fig. 3a. For clarity and better comparison, the representative thermo-Raman spectra recorded at 25 and 800 °C are shown in Fig. 3b. The spectra at 25 °C show a distinct band at 1309 cm^{-1} and weak broad bands at 1023, 807, 411, 370 and 326 cm^{-1}. The distinct band at 1309 cm^{-1} can be attributed to the carbonates derived from nickel acetate [31], which disappears above 300 °C on decomposition of acetate groups. Strong background in the range 300–700 cm^{-1} is also observed, probably because of the hydrocarbons associated with nickel acetate, and hydrocarbons are known to contribute to the background [27,32]. The background eventually decreases with the decomposition of acetate groups around 300 °C, and is in agreement with TGA thermogram (Fig. 2) and the disappearance of the band at 1309 cm^{-1}. However, decomposition of acetate groups result in blackening of the sample surface and consequently poor scattering is observed till the surface is oxidized around 320 °C (spectrum not shown). With further increase in temperature to 400 °C, weak bands corresponding to NiO–Al_2O_3 start appearing while the background disappears. This indicates that the formation of NiO–Al_2O_3 starts at 400 °C and crystallinity develops with further rise in temperature above 600 °C, which is further justified by XRD data (vide infra). Increase in intensity of the bands corresponding to NiO–Al_2O_3 is observed as the temperature approaches 800 °C, and show bands at 1109, 1028, 950, 816, 703, 600 (weak), 497 and 376 cm^{-1}. Thermal broadening and sharpening of the supported nickel oxide Raman band is observed on heating the sample from 500 to 800 °C. This suggests that the nickel oxide vibrational modes may be intimately coupled to the vibrations of the alumina support. The Raman bands present in the region 900–1100 cm^{-1} clearly suggest that M=O bonds are present in NiO–Al_2O_3 system, while the presence of characteristic band at 497 cm^{-1} suggests the presence of crystalline NiO supported on alumina [33]. NiO has a defect NaCl structure with Ni in octahedral sites, and $NiAl_2O_4$ formed by the solid-state reaction between NiO and Al_2O_3 at elevated temperature has an inverse spinel structure with Ni in octahedral and tetrahedral sites [34]. The crystalline NiO generally exhibits two broad and overlapping Raman bands at 460 and 500 cm^{-1}, and crystalline $NiAl_2O_4$ possesses Raman bands located at 200, 375 and 600 cm^{-1} [35]. Thus, the weak bands observed at 600 and 376 cm^{-1} indicate the presence of small amount of crystalline $NiAl_2O_4$. Controversy still exists regarding the temperature at which $NiAl_2O_4$ is formed. Reports of calcination at 600 °C for the formation of $NiAl_2O_4$ exist, to which, Aminzadeh and Sarikhani-frad argue as Raman inactive γ-Al_2O_3 phase is formed at 600 °C [27]. However, thermo-Raman study indicates that the bulk $NiAl_2O_4$ is formed at temperatures above 800 °C, although the onset of formation is 600 °C and is a slow process.

Supported nickel oxide as investigated by Chan and Wachs [35] exhibited a Raman band at $\sim$550 cm^{-1} and did not possess the crystalline NiO Raman bands at 460 and 500 cm^{-1} or crystalline $NiAl_2O_4$ Raman bands at 200, 375 and 600 cm^{-1}. However, their XPS and XRD examination indicated that the nickel oxide was highly dispersed as Ni^{2+} on the alumina support. The presence of Raman band at 497 cm^{-1}, characteristic of crystalline NiO, suggests that the surface nickel oxide might be incorporated into the subsurface of the alumina as a surface spinel. This is supported by the fact that the low oxidation state of nickel oxide can be accommodated in the Al_2O_3 lattice and leads to the formation of NiO–Al_2O_3 spinels [34,36]. Cimino et al. [37] in their reflectance studies observed the incorporation of surface nickel oxide as Ni^{2+} ions in a spinel-like phase into the subsurface of the alumina support. Heating of NiO–Al_2O_3 sample to high temperatures might cause diffusion of the surface nickel oxide into the bulk of the alumina support transforming it to $NiAl_2O_4$ [38]. However, thermal process in the range from 25 to 800 °C apparently converted a small amount of the supported nickel oxide to $NiAl_2O_4$. Monitoring the solid-state reaction at temperatures above 800 °C would have been interesting, but was beyond the experimental limits of the instrumental setup.

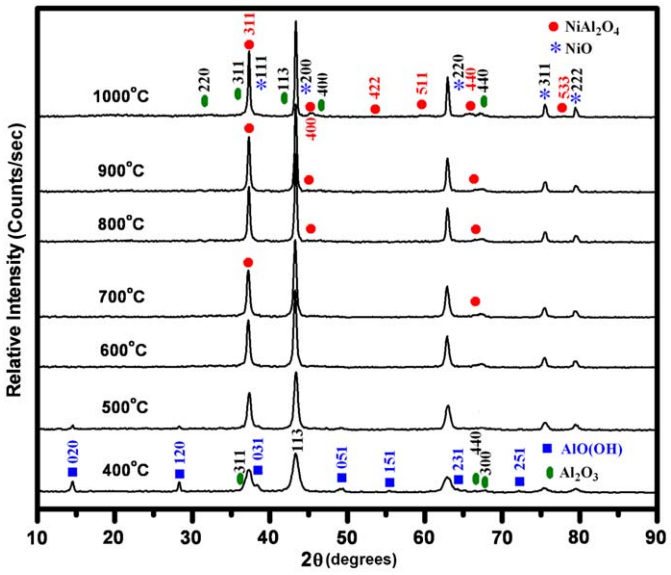

Fig. 4. X-ray diffraction patterns of solid-state mixture of $Ni(CH_3COOH)_2$ and $Al(OH)_3$ (molar ratio 1:2) as a function of temperature.

Earlier *in situ* Raman spectroscopic studies of supported metal oxides have revealed that there are two types of supported metal oxides on γ-Al_2O_3 based on adsorption and absorption [35]. Metal oxides with higher oxidation states generally adsorb on the surface of γ-Al_2O_3 as they cannot be accommodated, and usually possesses strong Raman bands at $\sim$900–1100 cm^{-1}. The metal oxides with low oxidation states can be absorbed into the surface of the alumina support as a surface spinel, owing to their accommodation in the γ-Al_2O_3, and usually possess Raman bands at $\sim$300–800 cm^{-1}. Thus, Raman bands observed at 1028 and 1109 cm^{-1} can be unambiguously assigned to the symmetric stretching mode of short

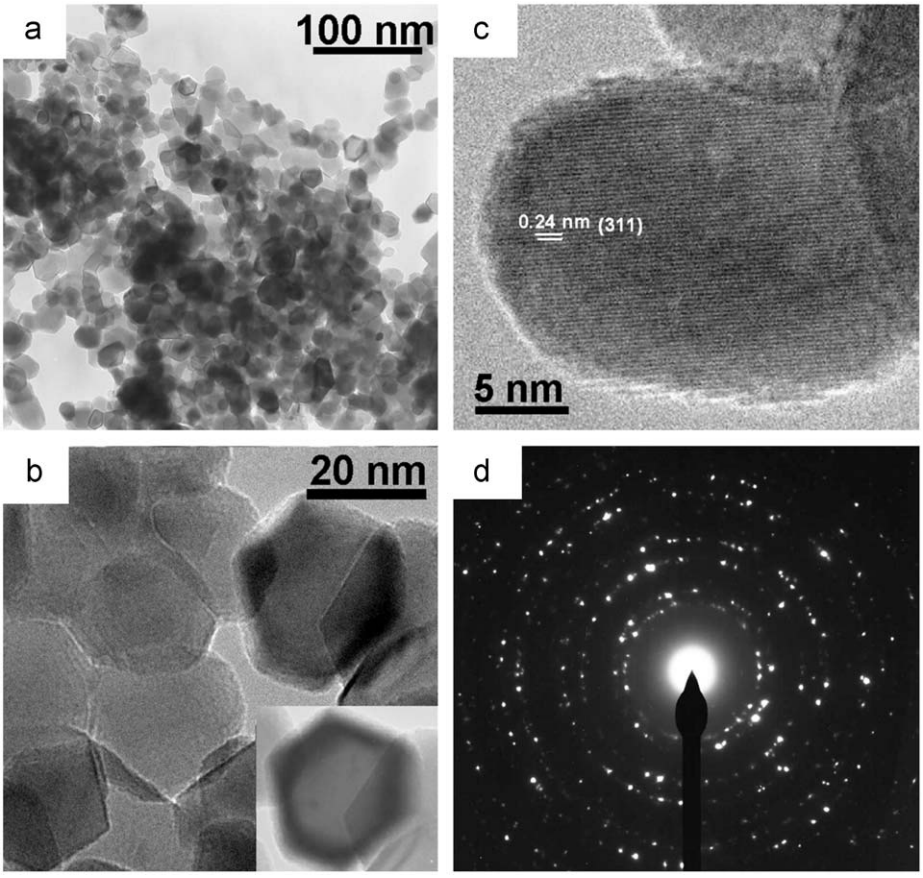

Fig. 5. (a–b) Representative TEM images of NiO–Al_2O_3 (solid-state reaction) heated at 800 °C under controlled heating conditions at the rate of 5 °C min^{-1}. Inset in (b) shows image of a single NiO–Al_2O_3 particle. The particle size observed is 20–30 nm. (c) HRTEM image of single NiO–Al_2O_3 nanoparticle showing lattice fringes with lattice spacing of 0.24 nm (311). (d) Representative SAED pattern of NiO–Al_2O_3 nanoparticles.

terminal M═O bonds (i.e., ν_s [M═O]), whereas Raman bands at 950 and 816 cm^{-1} can be attributed to either the antisymmetric stretch of M–O–M bonds (i.e., ν_{as}[M–O–M]) or the symmetric stretch of (–O–M–O–)n bonds (i.e., ν_s[(–O–M–O–)$_n$]) characteristic of absorbed metal oxides [39]. The relatively broad band at 950 cm^{-1} is likely due to the co-existence of terminal M═O bands and a variety of M–O polymeric species. In this study, Raman bands in the range 300–1100 cm^{-1} were observed suggesting the presence of NiO species being adsorbed and absorbed in the alumina support. This is probably due to higher Ni:Al_2O_3 ratio used in this experiment compared to earlier report where 13% Ni was used [35].

Based on the thermo-Raman experiments, it is understood that the formation of NiO–Al_2O_3 starts around 400 °C. Thus, diffraction patterns from the solid-state reaction mixture heated to 400, 500, 600, 700, 800, 900 and 1000 °C were recorded and are presented in Fig. 4. The XRD patterns observed from the solid-state mixture show sharp peaks with narrow band-width, which indicates that NiO–Al_2O_3 nanoparticles have good crystallinity. No significant difference between diffraction patterns of samples is noted, except for the change in intensity. The average particle size calculated from Scherrer formula is ~25 nm, which is in good agreement with that observed in TEM images. The XRD pattern at 400 °C show peaks corresponding to AlO(OH) (JCPDS card 21-1307), Al_2O_3 (JCPDS card 11-0661 and 10-0425), NiO (JCPDS card 47-1049) and $NiAl_2O_4$ (JCPDS card 10-0339) supporting the formation of NiO–Al_2O_3. At higher temperatures above 600 °C, less intense peaks corresponding to $NiAl_2O_4$ (JCPDS card 10-0339) start appearing and the intensity increases as the temperature approaches 1000 °C. This indicates the formation of $NiAl_2O_4$ in the subsurface of the alumina as a result of diffusion. The formation of $NiAl_2O_4$ from NiO and Al_2O_3 is a slower process than the diffusion of Ni in Al_2O_3 and this may delay the change in lattice parameters and overall composition of the material.

TEM images of NiO–Al_2O_3 nanoparticles obtained from solid-state mixture heated to 800 °C at the rate of 5 °C min^{-1} are shown in Fig. 5. The particle size diameter as observed from the TEM images is 20–30 nm and the morphology of the particles varied from spherical to hexagonal shape (inset of Fig. 5b). Well-crystallized particles with minimum to no aggregation were observed, probably because of the carbonaceous material produced during the decomposition of acetate groups preventing the aggregation. However, the carbonaceous material is lost subsequently during the thermal process and is justified from the disappearance of the Raman band at 1309 cm^{-1} in TRS study. The composition of the NiO–Al_2O_3 nanoparticles is confirmed from the EDS spectra showing presence of Ni, Al, and O (data not shown) with Ni:Al ratio of 28:72. Slightly low content of Ni in solid-state reaction mixture can be attributed to the loss of nickel as nickel acetate, during thermal decomposition process. High resolution TEM image of single NiO–Al_2O_3 nanoparticle obtained from solid-state reaction clearly shows the lattice fringes with the lattice spacing of 0.24 nm as shown in Fig. 5c. This supports the crystalline nature of the obtained NiO–Al_2O_3 nanoparticles. SAED pattern obtained from the nanoparticles of same sample showed ring pattern with discrete bright spots revealing a typical well-crystallized diffraction pattern of NiO–Al_2O_3 as shown in Fig. 5d.

SEM images of NiO–Al_2O_3 obtained from samples at selected different temperatures from solid-state reaction are shown in Fig. 6. Large particles and clusters were observed in the sample at lower temperature reflecting poor crystalline nature. However, the crystallinity improved with rise in temperature above 400 °C. Uniform distribution of the nanoparticles size (20–30 nm) is observed in the temperature range from 600 to 800 °C as shown in Figs. 6b and c, but showed aggregation as the temperature increased to 1000 °C (Fig. 6d). This phenomenon along with decrease in surface area of the catalyst was also observed by

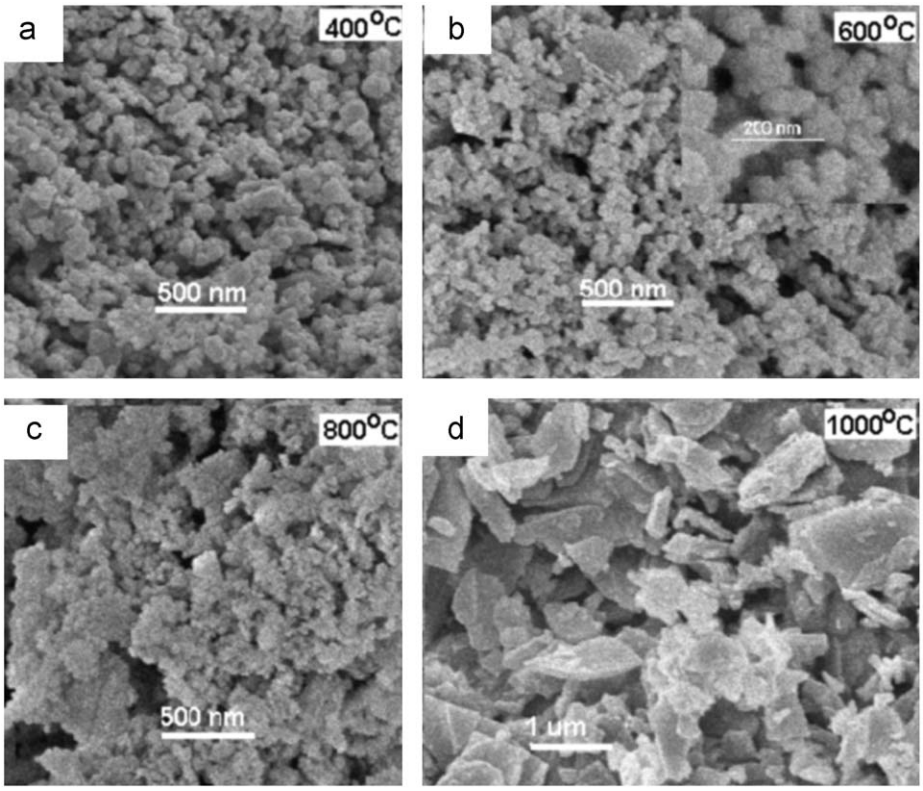

Fig. 6. SEM images of NiO–Al_2O_3 nanoparticles obtained from solid-state reaction of $Ni(CH_3COOH)_2$ and $Al(OH)_3$ (molar ratio 1:2) as a function of temperature; (a) 400 °C, (b) 600 °C, (c) 800 °C, and (d) 1000 °C. Inset in (b) shows magnified image of the NiO–Al_2O_3 nanoparticles.

Twigg et al. [40] in their studies. As particle size and size distribution is important for catalytic property, calcination at 600–800 °C would be ideal for $NiO–Al_2O_3$ catalyst preparation using solid-state mixture.

4. Conclusion

In this work, utility of hyphenated thermogravimetric analyzer and TRS has been shown for monitoring the dynamic thermal process of $NiO–Al_2O_3$ catalyst formation from solid-state reaction with controlled heating at the rate of 5 °C min^{-1}. TGA-DTG data were in harmony with the thermo-Raman data. Monitoring the thermal processes by TRS provides useful and direct structural information compared to other conventional techniques, which provides limited information. Furthermore, it was observed that the solid-state reaction produces well-crystallized $NiO–Al_2O_3$ nanoparticles at lower temperature and is supported by the XRD data. The $NiO–Al_2O_3$ obtained in the solid-state reaction has uniform size distribution of ~20–30 nm in diameter. This was supported by complementary characterizations using XRD, TEM, and SEM. Based on our thermo-Raman and microscopy studies, it has been observed that calcination at 600 °C is enough to produce $NiO–Al_2O_3$ catalyst, however, higher temperatures can be used to improve the crystallinity. TRS studies also revealed that the bulk $NiAl_2O_4$ forms at temperatures above 800 °C although the onset of formation is around 600 °C. Furthermore, this study unambiguously demonstrates the utility of the hyphenated thermogravimetric analyzer and TRS to monitor the thermal processes that are of a crucial research and industrial significance.

Acknowledgments

Financial support by National Science Council (NSC94-2218-E-007-052 and NSC95-2113-M-007-044-MY3) and National Tsing Hua University are gratefully acknowledged.

References

[1] B.K. Hodnett, F.J.J.G. Janssen, J.W. Niemantsverdriet, V. Ponec, R.A. van Santen, J.A.R. van Veen, Catalysis: An Integrated Approach, Elsevier, Amsterdam, 1999.
[2] A. Becerra, M. Dimitrijewits, C. Arciprete, A.C. Luna, Gran. Matter 3 (2001) 79–81.
[3] Y. Cesteros, P. Salagre, F. Medina, J.E. Sueiras, Chem. Mater. 12 (2000) 331–335.
[4] P.H. Bolt, F. Habraken, J.W. Geus, J. Solid State Chem. 135 (1998) 59–69.
[5] Y. Cesteros, P. Salagre, F. Medina, J.E. Sueiras, Appl. Catal. B 25 (2000) 213–227.
[6] J.S. Choi, K.I. Moon, Y.G. Kim, J.S. Lee, C.H. Kim, D.L. Trimm, Catal. Lett. 52 (1998) 43–47.
[7] J.H. Fei, Z.Y. Hou, X.M. Zheng, T.S. Yashima, Catal. Lett. 98 (2004) 241–245.
[8] E. Avendano, A. Azens, G.A. Niklasson, C.G. Granqvist, Sol. Energy Mater. Sol. Cells 84 (2004) 337–350.
[9] J.J. Vijaya, L.J. Kennedy, G. Sekaran, K.S. Nagaraja, Mater. Lett. 61 (2007) 5213–5216.
[10] O. Abe, S. Takata, Y. Ohwa, J. Eur. Ceram. Soc. 24 (2004) 489–494.
[11] G.H. Li, L.J. Hu, J.M. Hill, Appl. Catal. A 301 (2006) 16–24.
[12] J.A. Azurdia, J. Marchal, P. Shea, H.P. Sun, X.Q. Pan, R.M. Laine, Chem. Mater. 18 (2006) 731–739.
[13] M.M. Amini, L. Torkian, Mater. Lett. 57 (2002) 639–642.
[14] E. Loginova, F. Cosandey, T.E. Madey, Surf. Sci. 601 (2007) L11–L14.
[15] V.G. Kessler, G.A. Seisenbaeva, S. Parola, J. Sol–Gel Sci. Technol. 31 (2004) 63–66.
[16] P. Jeevanandam, Y. Koltypin, A. Gedanken, Mater. Sci. Eng. B 90 (2002) 125–132.
[17] C. Weidenthaler, W. Schmidt, Chem. Mater. 12 (2000) 3811–3820.
[18] M. Houalla, F. Delannay, B. Delmon, J. Phys. Chem. 85 (1981) 1704–1709.
[19] C.H. Bartholomew, Appl. Catal. A 107 (1993) 1–57.
[20] S.E. Wanke, P.C. Flynn, Catal. Rev. 12 (1975) 93–135.
[21] P. Desai, J.T. Richardson, Catalyst Deactivation, Elsevier, Amsterdam, 1980.
[22] J.T. Richardson, R.M. Scates, M.V. Twigg, Appl. Catal. A 267 (2004) 35–46.
[23] P. Forzatti, L. Lietti, Catal. Today 52 (1999) 165–181.
[24] T. Arunarkavalli, Proc. Indian Acad. Sci.-Chem. Sci. 108 (1996) 27–37.
[25] L.W. Burggraf, D.E. Leyden, R.L. Chin, D.M. Hercules, J. Catal. 78 (1982) 360–379.
[26] J.R. Bartlett, R.P. Cooney, Spectroscopy of Inorganic-based Material: Raman Spectroscopic Studies in Chemisorption and Catalysis, Wiley, New York, 1987.
[27] A. Aminzadeh, H. Sarikhani-fard, Spectrochim. Acta A 55 (1999) 1421–1425.
[28] K.D. Becker, Solid State Ionics 141 (2001) 21–30.
[29] A.V. Ghule, B. Lo, S.H. Tzing, K. Ghule, H. Chang, Y.C. Ling, Chem. Phys. Lett. 381 (2003) 262–270.
[30] A. Ghule, S.H. Tzing, J.Y. Chang, K. Ghule, H. Chang, Y.C. Ling, Eur. J. Inorg. Chem. (2004) 1753–1762.
[31] R.L. Frost, W. Martens, Z. Ding, J.T. Kloprogge, T.E. Johnson, Spectrochim. Acta A 59 (2003) 291.
[32] A. Aminzadeh, Appl. Spectrosc. 51 (1997) 817–819.
[33] I.R. Beattie, T.R. Gilson, J. Chem. Soc. A (1969) 2322–2327.
[34] A.F. Wells, Structural Inorganic Chemistry, fifth ed., Oxford University Press, Oxford, 1984.
[35] S.S. Chan, I.E. Wachs, J. Catal. 103 (1987) 224–227.
[36] P. Porta, F.S. Stone, R.G. Turner, J. Solid State Chem. 11 (1974) 135–147.
[37] A. Cimino, M. Lo Jacono, M. Schiavello, J. Phys. Chem. 75 (1975) 243–249.
[38] M. Akaogi, S.I. Akimoto, K. Horioka, K.I. Takahashi, H. Horiuchi, J. Solid State Chem. 44 (1982) 257–267.
[39] B.M. Weckhuysen, J.M. Jehng, I.E. Wachs, J. Phys. Chem. B 104 (2000) 7382–7387.
[40] M.V. Twigg, J.T. Richardson, Appl. Catal. A 190 (2000) 61.